Domain wall displacement is the origin of superior permittivity and piezoelectricity in $BaTiO_3$ at intermediate grain sizes

Dipankar Ghosh,[1,3] Akito Sakata,[1] Jared Carter,[1] Pam A. Thomas,[4] Hyuksu Han,[1] Juan C. Nino[1] and Jacob L. Jones[1,2*]

[1]*Department of Materials Science and Engineering, University of Florida, Gainesville, FL 32611, USA*

[2]*Department of Materials Science and Engineering, North Carolina State University, Raleigh, NC, 27695, USA*

[3]*Division of Engineering and Applied Science, California Institute of Technology, Pasadena, CA 91125, USA*

[4]*Department of Physics, University of Warwick, Coventry, CV4 7AL, UK*

Keywords: Barium titanate, grain size, piezoelectricity, permittivity, *in situ* X-ray diffraction, domain wall motion.

*Corresponding Author: email jacob_jones@ncsu.edu, telephone 352-846-3788

Abstract

The dielectric and piezoelectric properties of ferroelectric polycrystalline materials have long been known to be strong functions of grain size and extrinsic effects such as domain wall motion. In $BaTiO_3$, for example, it has been observed for several decades that the piezoelectric and dielectric properties are maximized at intermediate grain sizes (~1 μm) and different theoretical models have been introduced to describe the physical origin of this effect. Here, using *in situ*, high-energy X-ray diffraction during application of electric fields, we show that 90° domain wall motion during both strong (above coercive) and weak (below coercive) electric fields is greatest at these intermediate grain sizes, correlating with the enhanced permittivity and piezoelectric properties observed in $BaTiO_3$. This result validates the long-standing theory of Arlt *et al.* in attributing the size effects in polycrystalline $BaTiO_3$ to domain wall displacement. It is now empirically established that a doubling or more in the piezoelectric and dielectric properties of polycrystalline ferroelectric materials can be achieved through domain wall displacement effects; such mechanisms are suggested for use in the design of new ferroelectric materials with enhanced properties.

1. Introduction

Size effects in ferroic materials are of fundamental importance and play a crucial role in the functionality of devices at increasingly smaller length scales [1-5]. In polycrystalline ferroelectrics, size effects are chiefly evident in materials properties such as the relative dielectric permittivity (ε_r) and piezoelectric coefficients (e.g., d_{33} and d_{31}). For polycrystalline barium titanate ($BaTiO_3$), the effect of grain size on the relative permittivity has been extensively reported over the past decades [3,4,6-20] and is of particular relevance to the continuous size reduction of $BaTiO_3$ capacitors. Within the grain size range of 1-10 μm, it is now widely accepted that ε_r of polycrystalline $BaTiO_3$ increases with decreasing grain size, reaching a value of 5000, or higher, as the grain size approaches 1 μm. Below 1 μm, however, ε_r of $BaTiO_3$ decreases markedly with further decreasing grain size. The superior ε_r values of $BaTiO_3$ at an intermediate grain size of approximately 1 μm exceed those measured in $BaTiO_3$ single crystals ($\varepsilon_{[100]}$=4000; $\varepsilon_{[001]}$=170) [7] and, furthermore, cannot be explained by orientational averaging of the single crystal anisotropic permittivity values. Limited studies have also shown comparable increases in the piezoelectric coefficients, d_{33} or d_{31}, at intermediate grain sizes near 1 μm [6,21].

Two widely known theories attribute the origin of the superior relative permittivity in polycrystalline $BaTiO_3$ at intermediate grain sizes to either an *internal residual stress* that changes the domain architecture and increases the intrinsic contribution [5,7,8,22] or *enhanced motion of 90° domain walls* resulting in increased extrinsic contribution [9,10,11,19]. A complete and quantitative separation of the effects of internal stress and domain wall dynamics as a function of grain size is yet to be provided. This knowledge gap is primarily attributed to the lack of *in situ* crystallographic or microstructural investigations during application of applied electric fields. Such *in situ* studies can uniquely measure the dynamics and mechanics of

domains as a function of grain size as well as provide insight into the internal stress states of materials. Here, we undertake such measurements using an *in situ* high-energy X-ray diffraction (XRD) technique in transmission geometry during application of external electric fields of strong amplitude (above the ferroelectric coercive field, E_c) and weak amplitude (below E_c). This technique reveals the time-resolved crystallographic changes in $BaTiO_3$ as a function of grain size during electric field application.

High-energy X-rays are particularly beneficial in the study of ferroelectric polycrystalline materials because they can penetrate entire mm-sized samples, meaning the measured diffraction patterns can be said to capture the average behavior of all crystallites in the polycrystalline aggregate, which is a necessary requirement for making quantitative structure-property relationships. In polycrystalline ferroelectrics prior to electric field application, there is no preferred orientation of grains or domains. A preferred domain texture evolves during electric field application as a fraction of the non-180° ferroelectric/ferroelastic domains reorient towards a more preferred direction relative to the applied field [23]. During this domain reorientation, crystallographic and microstructural effects as a result of electric-field-induced lattice strain and domain wall motion can be measured using X-ray and neutron diffraction [24-31]. Domain reorientation, specifically, can be quantified using the intensity interchange between the different orientation variants. Thus, diffraction provides one route to assess the two competing theories described above and will help to understand the structural origin of grain size effects in $BaTiO_3$.

Using this *in situ*, high-energy XRD technique across the grain size range of 0.2 μm to 3.5 μm, we show conclusive and direct evidence that 90° domain wall motion in $BaTiO_3$ is present during both strong and weak field amplitudes (*i.e.*, corresponding to field amplitudes significantly above and below the macroscopic ferroelectric coercive field). Most importantly,

domain wall motion reaches a maximum at a grain size of ~2 μm where the relative permittivity and piezoelectric coefficient are also maximized. Additionally, measurement of the unit cell volume and spontaneous lattice strain prior to electric field application evidences that the change in residual internal stress across this grain size range is small. We therefore conclusively attribute 90° domain wall motion to the superior properties in $BaTiO_3$ of intermediate grain sizes (~1-2 μm). Moreover, the *in situ* measurements reveal, unexpectedly, that application of strong electric field amplitudes triggers an additional reversible phase transition through internal elastic interaction, which is most apparent in the coarse-grained $BaTiO_3$ ferroelectrics.

2. Results and Discussion

2.1. Permittivity and piezoelectric coefficient as a function of grain size

Using both spark plasma sintering (SPS) [32,33] and conventional pressureless sintering, polycrystalline $BaTiO_3$ of six different grain sizes were synthesized. The average grain sizes ranged from ~0.2 to 3.5 μm (**Figure 1**(a)), which span the behavioral regimes introduced earlier. The grain size distributions are provided in the supporting information. Annealing was also undertaken on all samples in flowing oxygen in order to mitigate residual stresses and oxygen non-stoichiometry of the samples; this procedure is described in the experimental section and additional information is provided in supporting information. **Figure 1**(b) presents both the relative permittivity (ε_r) and the direct longitudinal piezoelectric coefficient (d_{33}) of the synthesized polycrystalline $BaTiO_3$ samples at room temperature. Within the investigated grain size range, ε_r is observed to be maximum (>5000) at ~2 μm and values of ε_r decrease both above and below this grain size, which agrees with previously reported trends [3,4,9,10,11]. The permittivity was also measured as a function of temperature up to temperatures exceeding the

Curie temperature (T_c) and the response at 1 kHz is reported in the supporting information. The T_c remains nearly constant for all grain sizes and the associated loss increases slightly with decreasing grain size as expected. The longitudinal piezoelectric coefficients (d_{33}) measured on the same samples reveal a similar trend with room temperature d_{33} reaching a maximum at the grain size of ~2 μm.

2.2. Previous theoretical models

Before proceeding, we briefly review the two theories of superior permittivity in ferroelectric $BaTiO_3$ at grain sizes of ~1-2 μm, specifically the models of residual stress and 90° domain wall contribution. The phenomenological residual stress model attributes the observed peak in ε_r at approximately 1 μm grain size in polycrystalline $BaTiO_3$ to an increased internal residual stress at this grain size [5,7,8,22]. This internal residual stress is said to arise during the paraelectric cubic to ferroelectric tetragonal phase transition at the Curie temperature [5,7,8,22,34] and is relieved to some extent due to formation of the ferroelectric/ferroelastic tetragonal domains within each single grain of $BaTiO_3$ at room temperature. At grain sizes close to 1 μm, it was originally argued that the 90° domain walls do not form and therefore, the internal residual stress is not as relieved as the larger grain sizes. This residual stress is then thought to suppress the tetragonality of the $BaTiO_3$ lattice thus retaining a structure closer in proximity to the cubic state. Since the relative permittivity of $BaTiO_3$ is significantly higher in states nearer the T_c compared to that at room temperature, a sharp increase in ε_r would be observed at grain sizes close to 1 μm [5,7,8,22]. This argument was largely disputed in Frey and Payne by showing that T_c was nearly constant with grain size for samples synthesized by a sol-gel method [35].

After the existence of 90° domain walls was later revealed below 1 μm [9,10,11], Arlt *et al.* [9] introduced an alternate model which attributes the superior permittivity in polycrystalline $BaTiO_3$ of intermediate grain size to 90° domain walls. In this model, the permittivity increases from grain sizes of 10 μm down to grain sizes of ~1 μm due to an increase in 90° domain wall density. In this model, it was assumed that the contribution of domain walls was due to their displacement or motion during perturbation; it was much later that the intrinsic response of domain walls themselves were clearly observed to enhance property coefficients (e.g., as shown by Wada *et al.* in $BaTiO_3$ single crystals [36]). In the original model by Arlt *et al.*, it was also assumed that the force constant for 90º domain wall displacement is independent of domain width. Later, Arlt and Pertsev [37,38] calculated a domain width dependence of the force constant that changed between coarse-grained microstructures (banded domain structure wherein each band has a regular laminar structure) and finer-grained microstructures (regular laminar domain structure). According to these calculations, the force constant is higher in fine-grained microstructures than in coarse-grained microstructures. As a result, domain walls in thinner domain structures are more difficult to move than domain walls in thicker domain structures. Due to the stiffer force constant predicted in $BaTiO_3$ of smaller grain size, Arlt and Pertsev [37] suggested that the higher permittivity at grain sizes near 1 μm may not be caused by the high density of 90º domain walls as was suggested earlier [9]. However, it was also rationalized that as the grain size decreases towards 1 μm, a strong softening of the force constant may be expected owing to the reduction of stresses in and near the grain boundary areas. This, in turn, may act as a feedback and ultimately enhance the domain wall contribution in grain sizes of ~1 μm [37].

Below a grain size of ~1 μm, the decrease in permittivity is considered to arise from both the lowering of 90° domain wall density and restricted domain wall motion. These effects thus reduce the contribution of 90° domain walls to relative permittivity. Damjanovic [39] supported these observations by showing that activity of domain walls becomes weaker in $BaTiO_3$ of finer grain size (0.7 μm) than in $BaTiO_3$ of coarser grain size (26 μm) because the domain walls are relatively more clamped in the former than in the latter. For even smaller grain sizes below 300-500 nm, the grain size starts to become comparable to the size of a single domain. As a result, the domain wall displacement and nucleation of new domains become more difficult under application of electric fields or stress [3,4]. Direct experimental measures of the grain size dependence of domain wall motion and its contribution to macroscopic property coefficients is needed in order to reconcile these various effects, in particular in a range of grain sizes that transcend the 1-2 μm grain size range of enhanced property coefficients (e.g., **Figure 1**(b)).

2.3. Structural changes and residual stress as a function of grain size

High-energy XRD patterns of the {200} and (111) Bragg reflections measured prior to electric field application are shown in Figs. 2(a) and 2(b), respectively. These diffraction patterns indicate some systematic structural changes with grain size. **Figure 2**(a) shows extremely weak splitting of the (002) and (200) Bragg reflections in the smallest grain size (~0.2 μm) and the extent of splitting increases with increasing grain size. The (200) peak positions (related to the ***a*** lattice parameter) remain almost constant with increasing grain size whereas the (002) peak position (related to the ***c*** lattice parameter) shifts consistently to higher lattice spacing (lower 2θ) as the grain size increases. Additionally, increased diffuse scattering or additional X-ray intensity between the (002) and (200) Bragg reflections is observed with decreasing grain size. This

increase in the diffuse scattering may suggest either that the density of domain walls increases with grain size reduction (e.g., as reviewed in Ref. [40]) and/or that the strain field surrounding the 90º domain walls increases in the smaller grain sizes [10,41,42]. As the density of domain walls is clearly a defining variable to property coefficients in single crystal $BaTiO_3$ [36], it is tempting to speculate that an increase in domain wall density (as may be indicated in the present work by the increased diffuse scattering) may lead to increased property coefficients. However, the dielectric and piezoelectric coefficients do not correlate proportionally to the diffuse scattering, instead maximizing at ~2 μm. Thus, the domain wall density in and of itself is insufficient to explain the observed superior properties at ~2 μm. Finally, **Figure 2**(b) shows some systematic changes in the (111) Bragg reflection with grain size variation, though the differences are less pronounced than in the {200} reflections. In the grain sizes of ~0.2 and 0.3 μm, the peak broadening of the (111) reflection relative to the larger grain sizes is most pronounced.

To quantify the structural changes in $BaTiO_3$ as a function of grain size, lattice parameters (***c*** and ***a***), lattice aspect ratio (***c***/***a***), unit cell volume, and full width at half maximum (FWHM) were further evaluated. The lattice parameters were determined from the (002) and (200) Bragg reflections, and subsequently used to calculate the ***c***/***a*** and unit cell volume (***a***×***a***×***c***). The (002) and (200) Bragg reflections were fitted with the pseudo-Voigt profile shape function and the lattice parameters were determined from the central peak positions of the fitted profiles [42]. FWHM values reported here were determined from the (111) reflections because of their reduced sensitivity to diffuse scattering from domain walls relative to the {002} Bragg reflections. The FWHM values were determined by fitting the profile to a Pearson VII-type profile shape function. These respective profile shape functions were empirically found to best

describe the respective measured diffraction profiles. Examples of fitted profiles are shown in supporting information.

Figure 3(a) shows the changes in lattice parameters with grain size. Using these lattice parameters, the ***c***/***a*** and unit cell volumes (**Figures 3**(b-c), respectively) are useful in assessing the dependence of spontaneous ferroelastic strain and residual stress on grain size. The decrease in the ***c***/***a*** (**Figure 3**(b)) with decreasing grain size indicates that $BaTiO_3$ becomes less tetragonal at smaller grain sizes, which is consistent with earlier reports [3,9,43,44]. Notably, however, the asymmetric {200} diffraction profile of the smallest grain size material (~0.2 μm) shows that the tetragonal phase is still retained. In contrast, the unit cell volume (**Figure 3**(c)) remains almost constant across the entire grain size range of ~0.2 to 3.5 μm.

Figure 3(d) shows the FWHM values of the (111) Bragg reflection as a function of grain size. Among all the grain sizes, the largest FWHM is observed at the smallest grain size of ~0.2 μm and decreases with increasing grain size though the changes become less significant in the largest grain sizes. The observed broadening of the (111) Bragg reflection at grain sizes of ~0.2 and 0.3 μm can be attributed to either a crystallite size effect and/or increased microstrain relative to $BaTiO_3$ of larger grain sizes. Microstrain is described with a change in the distribution of lattice spacings; in contrast, a change in the average lattice plane position, or macrostrain, would be observed as shifts in the Bragg peak(s) and would be a measure of residual stress. The (111) peak positions are nearly independent of grain size, indicating that the macrostrain remains almost constant over the entire grain size range of ~0.2-3.5 μm. This observation from the (111) Bragg peaks is consistent with the observation from the {002} Bragg peaks that the unit cell volume (**Figure 3**(c)) remains approximately constant.

As discussed before, the phenomenological residual stress theory attributes the presence of a large residual stress to the sharp increase in the relative permittivity of $BaTiO_3$ in grain sizes of approximately 1-2 μm. Since the ε_r is observed to be maximum at ~2 μm in the present work (**Figure 1**), the phenomenological residual stress theory would suggest that residual stress should be maximum at this grain size. Observations presented thus far from XRD patterns obtained prior to electric field application (Figs. 2(b) and 3(d)), however, do not show a significant variation in residual stress across the grain size range of 1-3.5 μm. In contrast, the X-ray measurements may indicate a higher level of microstrain at grain sizes of ~0.2 and 0.3 μm, though these grain sizes exhibit lower relative permittivity and piezoelectric coefficients. Therefore, the observed increase in the relative permittivity and piezoelectric coefficient at the grain size of ~2 μm cannot be reconciled by the residual stress theory.

2.4. *In situ* X-ray diffraction during strong electric field application

In order to measure the electric field-induced structural changes in polycrystalline $BaTiO_3$, high-energy XRD measurements were undertaken on samples across the grain size range of ~0.2-3.5 μm. Since the high-energy X-rays can penetrate a large volume of material, high-energy XRD effectively measures the collective effect of the microscopic displacements of domain walls. These measurements are therefore utilized to interpret the effect of domain wall motion on the macroscopic property coefficients [26,30,45].

2.4.1. 90^o domain wall motion during strong electric field application

The structural response of ferroelectric $BaTiO_3$ to strong electric field amplitudes, or amplitudes exceeding E_c, is first presented. XRD patterns near the {200} diffraction profile are used to show the extent of domain wall motion during a bipolar electric field (±2.5 kV/mm) of

triangular waveform. These results are shown in **Figure 4** for three different grain sizes of 0.3, ~2, and ~3.5 μm which represent typical behaviors measured in the grain size regimes below 1 μm (**Figure 4**(a)), near 1-2 μm (**Figure 4**(b)), and above 2 μm (**Figure 4**(c)), respectively. Additional measurements for other grain sizes are provided in the supporting information. It can be seen in **Figure 4** that all of the measured grain sizes exhibit an exchange of intensity in the (002) and (200) Bragg reflections during electric field application. It is important to note that intensity interchange in these reflections of perovskite ferroelectrics has been shown to be indicative of 90° domain reorientation [26,30]. The present measurements therefore reveal direct evidence of 90° ferroelectric/ferroelastic domain wall motion during electric fields of high amplitude in polycrystalline $BaTiO_3$ for all the grain sizes investigated.

Representative X-ray line patterns measured at several specific states of the electric field waveform are further shown in the supporting information and highlight the quantitative changes in the diffraction patterns as a function of grain size and electric field amplitude and history. For the 0.3 μm grain size (**Figure 4**(a)), the XRD data indicates that the intensities of the (002) and (200) reflections increase and decrease, respectively, with increasing field magnitude during both polarities of the field. It is also observed that the (200) peak position remains almost unchanged during the electric field application while the (002) peak position shifts to higher 2θ (or lower *d*) with increasing electric field during both the positive and negative waveforms. For the ~2 μm grain size (**Figure 4**(b)), a dramatic change in the (002) and (200) peak intensities during electric field application is observed, which indicates a significantly enhanced 90° domain wall motion relative to that observed at the grain size of 0.3 μm. At a grain size of ~3.5 μm (**Figure 4**(c)), significant 90° domain wall motion is also observed, though to a lesser extent than at a grain size of ~2 μm.

Summarizing these observations from **Figure 4**, it is clear that significant 90° domain wall motion occurs during the bipolar high-field cycling at grain sizes of ~2 and ~3.5 μm whereas less 90° domain wall motion occurs at the smaller grain size of 0.3 μm. Thus, 90° domain wall motion is seen to increase with increasing grain size from 0.3 to ~2 μm, then decrease slightly with a further increase in the grain size to ~3.5 μm. These trends are consistent with the trends in ε_r and d_{33} introduced previously in **Figure 1**(b). The *in situ* X-ray measurements thus provide direct evidence of the grain size dependence of 90° domain wall motion which correlates with the increased property coefficients measured at ~2 μm. The observed results therefore support the theory attributing higher 90° domain wall contribution to the superior permittivity and piezoelectricity in $BaTiO_3$ at intermediate grain sizes.

2.4.2. Field-induced phase transition in $BaTiO_3$

The *in situ* X-ray measurements show an additional interesting structural feature during application of the highest electric field amplitudes in certain grain sizes (~2 and ~3.5 μm) - an additional Bragg reflection appears in between the (002) and (200) tetragonal phase reflections. These measurements indicate a field-driven polymorphic phase transition in $BaTiO_3$ during strong electric field amplitude. It is interesting to note that the observed phase transition becomes prominent near the maximum of the field amplitude (2.5 kV/mm) and subsequently disappears at zero field. The *in situ* X-ray measurements enable the observation of both the phase transition and its reversibility.

In order to further characterize the field-induced polymorphic state, the {200} composite diffraction profile is fit with three symmetric profile functions. Examples of resultant fits are shown in the supporting information. It can be seen that all the three Bragg reflections can be fit with three symmetric pseudo-Voigt profiles. This result could imply that the additional peak in

the middle of this diffraction profile is a single reflection, although any additional subtle peak splitting may not be resolved within the available instrumental resolution. The field-induced peak in the middle of the {002} diffraction profile is therefore interpreted as a different polymorphic phase of unknown symmetry.

Field-induced phase transitions in $BaTiO_3$ have been reported previously [46-50], and some of these studies [46-48] showed that the Curie temperature is shifted to higher values in the presence of an electric field, suggesting the proximity to a cubic phase decreases, or equally that the proximity to the orthorhombic phase increases. It is therefore possible that the field-induced phase is of orthorhombic symmetry. Further, other studies on $BaTiO_3$ single crystals [49,50] have reported an electric field-induced monoclinic phase close to the tetragonal-orthorhombic phase transition temperature. Once formed, this monoclinic phase is observed to be stable even upon removal of the field, a characteristic that is not observed in the present field-induced transition, though does not eliminate this phase from being the phase observed in the present work. It is also possible that the induced phase may be nonpolar (e.g., cubic) if the driving force is related to intergranular or other mechanical interactions within the grains.

Although the instrument resolution in the present work is not suitable for assigning a specific symmetry to this field-induced phase, some characteristics of this field-induced phase are worth noting in the present work. Though observed under both positive and negative polarity, the intensity of this new phase is consistently stronger under negative field amplitudes. Since this phase transition is observed at grain sizes in which the 90° domain wall motion is the greatest, it is considered that the structural origin of this phase transition is associated with the large strain of the polycrystalline aggregate and the extensive 90° domain wall motion in these grain sizes. The proposed structural origin is now discussed in more detail using the ~3.5 μm grain size

$BaTiO_3$ as a representative example (**Figure 4**(c), with specific profiles shown in supporting information in **Figure S6**(f)). At the maximum of positive and negative polarities, the (002) intensity is nearly constant, implying that the volume fraction of *c*-axis-oriented domains does not change significantly between the polarities. In contrast, a significant decrease in the (200) intensity is observed during the negative polarity relative to that during the positive polarity. This indicates that there is a further decrease in the volume fraction of the *a*-axis-oriented domains during the maximum of negative polarity relative to that during the maximum of positive polarity. This is unlike the typical (002) and (200) intensity interchange that is observed during domain reorientation of single phase tetragonal perovskites [23,26]. The observations for negative electric field polarity indicates that a fraction of the *a*-axis-oriented domains of the tetragonal phase change transform into the field-induced structure which exhibits the intermediate {002} diffraction peak.

A simplified schematic of this proposed mechanism is presented in **Figure 5**, which illustrates a simplified 90° domain configuration and the electromechanical strain interaction mechanism. In the initial state prior application of any electrical field (**Figure 5**(a)), the black rectangles represent domain orientation states within a single representative grain that are separated by 90° domain walls. During application of the electric field, strain is known to occur in ferroelectrics through 90° ferroelectric/ferroelastic domain wall motion and electric-field-induced distortion of the individual domains (e.g., piezoelectric strain). Within a single grain, these two mechanisms interplay and ultimately achieve an equilibrium response. It is further understood that domain wall motion within polycrystalline materials never results in a complete c-axis-oriented domain state due to intergranular mechanical constraints; remanent *a*-axis oriented domains remain in nearly all materials. These remanent *a*-axis oriented domains are

observed in the present experiments in the (200) intensity of the tetragonal phase. If the energy barrier for transition into an alternate polymorphic phase is low (e.g., due to the residual or induced stress state in polycrystals, proximity to the phase transition in temperature or composition, etc.), then it will be more favorable for the remanent *a*-axis-oriented domains to transform into this new ferroelastic strain state than for *c*-axis oriented domains. If *a*-axis-oriented domains transform into this new polymorph, then the strain of the transformed material will more closely parallel the effective strain of the crystal and polycrystalline aggregate.

The diffraction patterns for the other samples with grain sizes > 1 μm also show evidence that this field-induced, reversible phase transition may be present, though is not observed as clearly as in the sample with 3.5 μm grain size. The differences between different grain sizes may be a result of the crystal or domain sizes (which may affect the ability to observe the effect in diffraction), or there may exist a change in the expression of this effect in smaller grain sizes. Nevertheless, it is clear in the current *in situ* X-ray measurements that a reversible, field-induced phase transition is triggered during electric field amplitudes greater than the ferroelectric coercive field in coarse grained $BaTiO_3$ at room temperature.

2.4.3. *Determination of the extent of 90° domain reorientation*

Using diffraction, 90° domain wall motion in single-phase tetragonal ferroelectrics is traditionally quantified from changes in the volume fractions of the (002) and (200) orientation variants during electric field application. In the present work, a clear separation of the (002) and (200) diffraction intensities is not possible due to the presence of the field-induced polymorph at strong electric field amplitudes. We therefore introduce here a new method to associate changes in the {002} diffraction profile with the macroscopic strain of the sample. The method uses the cumulative diffraction intensity distribution of interplanar spacing, *d*, across the {002}

diffraction profile. The change in the median of this distribution can be used as a measure of the change in the type, proportions, and strain of {002} planes of a particular orientation in the sample. Thus, it is a measure of the combined effect of {002} lattice strains, 90° domain volume fractions (domain texture), and changes in phase fractions of coexisting polymorphs. For each cumulative intensity distribution, the median (d_{50}) is described by saying that ~50% of the material in the direction of the electric field has interplanar spacings above d_{50} and ~50% below d_{50}. Differences in structure factors of the tetragonal (002) and (200), and the {002} reflections of the induced polymorph may cause d_{50} to vary from a precise 50% indicator of volume fractions. Nevertheless, it is a useful quantitative metric for evaluating diffraction spectra with multiple overlapping peaks from multiple polymorphs.

Figure 6(a-c) shows XRD patterns measured prior to electric field application, at the maximum field amplitude (both positive and negative polarity), and the corresponding cumulative diffraction intensity distributions of interplanar spacing, d, for representative grain sizes 0.3, ~2 and ~3.5 μm. **Figure 6**(d) shows resulting changes in the d_{50} values before and during electric field application for these grain sizes. Several observations can be made from **Figure 6**(d). For all the grain sizes, the d_{50} values are higher during electric field application than prior to field application. This correlates with a positive electric-field-induced strain in {002}-oriented crystallites. Additionally, for each grain size, the d_{50} value during negative polarity is observed to be higher than that during positive polarity. The origin of this asymmetry is unknown, though asymmetries in strain behavior are often observed in ferroelectrics due to extrinsic effects [45]. Most importantly, **Figure 6**(d) indicates that change in d_{50} due to the electric field application is maximum at the grain size of ~2 μm. This means that the combined effect of {002} lattice strains, 90° domain volume fractions (domain texture), and changes in

phase fractions of coexisting polymorphs (tetragonal and the field-induced state) is observed to be maximum at the grain size of ~2 μm. Qualitatively, the observation of the {002} diffraction profiles (e.g., those in Figs. S5 and S6 of the supporting information) indicate that the dominant contribution to this behavior is from domain wall motion in the tetragonal phase which is observed in intensity interchanges between the tetragonal (002) and (200) reflections. Most notably, this grain size also exhibits the highest relative permittivity and piezoelectric coefficients as previously introduced in **Figure 1**(b).

2.5. *In situ* X-ray diffraction during weak electric field application

Having shown the structural response during strong electric fields, the structural response at weak electric field amplitudes is next examined. While application of electric fields above E_c results in large-scale domain wall motion (and, in certain grain sizes, a field-induced phase transition), small displacements of non-180° domain walls over local energy barriers at subcoercive field amplitudes (those below E_c) can be also measured using these X-ray approaches [30,45,51,52]. Such measurements provide a direct assessment of domain wall vibration (reversible) and small irreversible domain wall displacements at weak electric field strengths. Diffraction measurements at such weak fields can reveal the extrinsic contribution of domain wall motion to the property coefficients at conditions comparable to those used in the determination of macroscopic properties including relative permittivity and the piezoelectric coefficients [27,45,51,52]. Direct measurement of domain wall motion at weak field amplitudes can thereby provide further insight into the grain size dependence of 90° domain wall displacements and its relation to the relative permittivity and piezoelectric coefficient of $BaTiO_3$.

Figure 7(a-c) shows representative XRD profiles of 0.3, ~2, and ~3.5 μm grain sizes, measured using a square wave bipolar electric field of amplitude 0.2 kV/mm amplitude (approximately 40% of E_c). For each grain size, a subtle difference between the diffraction patterns measured at positive and negative polarities can be observed outside the error bars. This measurement of a very weak effect is made possible through the high intensities achievable at the synchrotron source. These results qualitatively indicate the presence of the 90° domain wall motion at very weak electric field strengths and are consistent with observations of similar effects in lead zirconate titanate (PZT) ceramics [53]. Notably, the intensity differences, and thus domain wall motion, is greatest for the ~2 μm grain size. In order to quantify domain wall motion due to electric field application, the measured diffraction profiles are fit to pseudo-Voigt shape functions to extract the integrated intensities of (002) and (200) peaks of the tetragonal $BaTiO_3$ phase. Even though the field-induced secondary polymorph is not observed during application of weak electric fields, a third peak is nevertheless required in order to adequately fit the {002} diffraction profiles measured at weak fields because diffuse scattering from 90° domain walls is observed between the tetragonal (002) and (200) reflections [42]. **Figure 7**(d) shows the calculated change in volume fraction of the two domain variants between the positive and negative polarities ($\Delta\eta_{002}$) as a function of grain size. This reveals an increase of the $\Delta\eta_{002}$ from the 0.3 μm grain size to the ~2 μm grain size followed by a continuing decrease in larger in grain sizes. The grain size dependence of 90° domain wall motion observed at weak field amplitude (**Figure 7**(d)) is consistent with the observations made at higher field amplitudes (**Figure 6**). That is, the *in situ* XRD measurements during both strong and weak electric field application show more domain wall displacement in the grain sizes in which the relative permittivity and piezoelectric coefficients are maximized.

2.6. Combined discussion

In polycrystalline ferroelectrics, the non-lattice extrinsic contribution to the macroscopic property coefficients (e.g., dielectric, piezoelectric and elastic) originates primarily from the collective motion of domain walls and other interfaces. Domain wall motion even at the weak to moderate fields (comparable to conditions where macroscopic property coefficients are measured) leads to the significant extrinsic contributions to the dielectric, elastic and piezoelectric property coefficients [30,31,54-59]. In many cases, this contribution may be comparable or greater than the intrinsic effect of the lattice itself [30,60,61]. The present work directly reveals that the motion of domain walls in $BaTiO_3$ is greatest at the intermediate grain sizes of ~2 μm, correlating with the maximum values of permittivity and piezoelectric coefficient. Quantitative evidence of this correlation exists from measurement of the response of the sample under both strong (d_{50}) and weak ($\Delta\eta_{002}$) field amplitudes.

With the insight obtained from the *in situ* XRD measurements, we return to the theories presented earlier that describe the origins of enhanced permittivity and piezoelectric coefficients at intermediate grain sizes on the order of ~1 μm. The phenomenological residual stress theory attributed the observed peak in ε_r at ~1 μm grain size to an increased internal residual stress [5,7,8,22]. However, the XRD measurements reveal no significant change in residual stress associated with macrostrain as a function of grain size. Thus, while residual stress may have a small effect, we do not observe it to be a dominant factor in the enhancement of relative permittivity and piezoelectric coefficients. The theory introduced by Arlt *et al.* [9,37,38] attributed the superior permittivity at intermediate grain sizes to the displacement of 90° domain walls in the tetragonal phase. The present *in situ* XRD measurements confirm the validity of this

theory under both strong and weak electric field amplitudes, i.e. that an enhanced displacement of 90° domain walls in grain sizes of ~1-2 μm leads to the enhanced relative permittivity and piezoelectric coefficients in $BaTiO_3$. Moreover, the observation of a reversible, field-induced polymorph in coarse-grained $BaTiO_3$ provides additional insight into the complexity of the micromechanics of polycrystalline ferroelectrics.

We previously showed that the piezoelectric coefficients in La-modified tetragonal PZT approaching the morphotropic phase boundary are dominantly (>50%) derived from the displacement of 90° domain walls [30]. The present work demonstrates both enhanced piezoelectric and dielectric properties in $BaTiO_3$ due to the displacement of domain walls. Holistically, the results of these experiments suggest that the displacement of domain walls and other extrinsic effects dominate the electromechanical response of real ferroelectric materials. Thus, the search for superior dielectric and piezoelectric properties of oxides should consider extrinsic effects as a source for enhanced response. In particular, the present search for superior piezoelectric coefficients in novel (both lead-containing and lead-free) perovskite compounds and solid solutions should consider the effect of domain wall motion to the realizable properties and material behavior. The present work demonstrated the ability to tune this enhanced response using grain size, though additional factors are known to affect domain wall mobility, notably through compositional modification such as donor doping. Theoretical models, including the ones introduced by Arlt *et al.* [9,37,38], may be further considered in exploiting these behaviors and properties in real materials.

3. Conclusions

In the current work, polycrystalline $BaTiO_3$ ceramics in the grain size range of ~0.2-3.5 μm were synthesized using conventional pressureless sintering and spark plasma sintering. Relative permittivity and longitudinal piezoelectric coefficient measurements showed that both the coefficients are maximum at approximately ~2 μm grain size. High-energy X-ray measurements prior to electric field application showed significant structural changes as a function of grain size in $BaTiO_3$, though did not indicate any significant variation of internal residual stress that can be attributed to the observed grain size effects. To study the effect of grain size on domain wall motion, samples were irradiated using high-energy X-rays during application of both strong and weak electric fields. These measurements revealed a strong dependence of grain size on domain wall motion which was observed to be maximum at approximately ~2 μm, the grain size in which the macroscopic property coefficients also maximize. Based on these results, we validate the theory of Arlt *et al.* in attributing the enhanced properties of $BaTiO_3$ to the displacement of domain walls. This knowledge should be used in the design of new materials with superior property coefficients and functionalities.

4. Experimental Section

4.1. Material synthesis, density measurements and microstructure

In the current work, $BaTiO_3$ ceramics of six different grain sizes across the grain size range of ~0.2-~3.5 μm were synthesized using spark plasma sintering (SPS) and conventional pressureless sintering of a commercially available nanocrystalline $BaTiO_3$ powder (Alfa Aesar, Ward Hill, MA) of approximate particle size of 50 nm (**Figure S1** in supporting information). Using SPS, $BaTiO_3$ ceramics of 0.21 μm and 0.3 μm grain sizes were synthesized. Other grain sizes (1.12 μm, 1.97 μm, 2.34 μm and 3.52 μm) of $BaTiO_3$ were synthesized using conventional

pressureless sintering. Details of the synthesis of these materials and all the sintering conditions are provided in the supporting information. Densities of the sintered materials were measured using Archimedes technique and the measured density values are listed in **Table S1** in supporting information. Average grain sizes of the sintered $BaTiO_3$ ceramics were estimated using lineal intercept technique in accordance with ASTM E112-10 standard test methods for determining average grain size and the grain size values are given in **Table S2** in supporting information. Grain size distributions of all the $BaTiO_3$ ceramics are shown in **Figure S2** in supporting information. Details of the sample preparation for the grain size measurements are also given in the supporting section. Microstructural analyses of the starting powder particles and sintered materials were performed using a field-emission scanning electron microscope (SEM, JEOL 6335F FEG-SEM).

4.2. Relative permittivity and piezoelectric measurements

The relative permittivity (ε_r) and longitudinal piezoelectric coefficient (d_{33}) measurements were conducted on $BaTiO_3$ samples after annealing in air. ε_r values of the $BaTiO_3$ were measured from room temperature to 200°C using an Agilent 4284A LCR meter in the frequency range of 1 kHz to 1 MHz in a temperature chamber and controller from Delta Design, Inc. For d_{33} measurements, the electroded specimens were placed in a silicone oil bath, poled under a DC field of 2.5 KV/mm at room temperature for 5 min and d_{33} values were measured using a d_{33} meter (YE2730A, APC Int. Ltd.). Procedures for specimen preparations for the ε_r and d_{33} measurements are given in the supporting information. All measured values are given in **Table S2**.

4.3. High-energy *in situ* XRD during strong and weak electric field application

To explore the grain size dependence of domain wall motion in $BaTiO_3$ ceramics and relation to bulk physical property coefficients, *in situ* high-energy XRD measurements during electric field application and in transmission geometry were conducted on the 11-ID-C beamline in the Advanced Photon Source (APS) at the Argonne National Laboratory. The high-energy XRD technique is capable of measuring the collective and average response of a large volume of the sample. *In situ* high-energy XRD during external electric fields enables investigation of crystallographic and microstructural changes in real time and macroscopic domain wall displacements can be quantified during the conditions at which properties and electromechanical behavior are characterized. The high energy of the X-ray beam (~110 keV) is highly penetrating and a wide coverage of reciprocal space is measured over a small angular scattering range. For each grain size $BaTiO_3$ sample, high-energy XRD patterns were measured initially on unpoled samples. Next, samples were electrically poled under bipolar electric fields of triangular waveform with a total time period of 60 seconds, with an effective frequency of ~0.02 Hz. Each sample was electrically poled using four successive electric field cycles of increasing magnitudes of ±1.0 kV/mm, ±1.5 kV/mm, ±2.0 kV/mm, and ±2.5 kV/mm. During every electric field application, the high-energy XRD patterns were recorded continuously in increments of 1 s exposure time. To investigate the domain wall motion at weak electric fields, *in situ* XRD measurements were also conducted at electric field strength of 0.2 kV/mm, which is below the macroscopic coercive field strength (approximately 0.5 kV/mm) of polycrystalline $BaTiO_3$ ceramics. The subcoercive *in situ* X-ray measurements were conducted on the electrically poled (after applying ± 2.5 kV/mm field) $BaTiO_3$ samples using an electric field of bipolar square wave form (± 0.2 kV/mm) at a frequency of 0.33 Hz. For each of the diffraction measurements, a large, representative volume fraction of a polycrystalline specimen was irradiated and XRD

patterns were measured at all angles relative to the applied electric field (**Figure S3** in supporting information).

Supporting Information

Supporting information is available from the Wiley Online Library or from the author.

Acknowledgements

This work was partially supported by the U.S. Department of the Army under contract number W911NF-09-1-0435, the U.S. National Science Foundation under award number DMR-0746902, and the Florida Cluster for Advanced Smart Sensor Technologies (FCASST) under "New Florida 2010". Use of the Advanced Photon Source was supported by the U. S. Department of Energy, Office of Science, Office of Basic Energy Sciences, under Contract No. DE-AC02-06CH11357. The authors gratefully acknowledge the help of Dr. Yang Ren and Dr. Guy Jennings at beamline 11-ID-C at the Advanced Photon Source and Prof. Ghatu Subhash for access to the SPS facilities. Also the authors acknowledge Dr. Shruti Banavara Seshadri and Dr. Goknur Tutunchu for help with *in situ* X-ray measurements and for helpful discussion.

References

1. Junquera, J. & Ghosez, P. Critical thickness for ferroelectricity in perovskite ultrathin films, Nature Mater, **422**, 506-509 (2003).
2. Dillon. D. F. et al. Ferroelectricity in ultrathin perovskite films, Science, **304**, 1650-1653 (2004).
3. Zhao, Z. et al. Grain-size effects on the ferroelectric behavior of dense nanocrystalline $BaTiO_3$ ceramics, Phys. Rev. B, **70**, 024107 (2004).
4. Buscaglia, M. T. High dielectric constant and frozen macroscopic polarization in dense nanocrystalline $BaTiO_3$ ceramics, Phys Rev B, **73**, 064114 (2006).
5. Martirenat, H. T. & Burfoot, J. C. Grain-size effects on properties of some ferroelectric ceramics, J. Phys. C: Solid State Phys. **7**, 3182-3192 (1974).
6. Zheng, P., Zhang, J. L., Tan, Y. Q., & Wang, C. L. Grain-size effects on dielectric and piezoelectric properties of poled $BaTiO_3$ ceramics, Acta Mater. **60**, 5022-5030 (2012).
7. Buessem, W. R., Cross, L. E. & Goswami, A. K. Phenomenological theory of high permittivity in fine-grained barium titanate, J. Am. Ceram. Soc. **49**, 33-36 (1966).
8. Buessem, W. R., Cross, L. E. & Goswami, A. K. Effect of two dimensional stress on the permittivity of fine- and coarse-grained barium titanate, J. Am. Ceram. Soc. **49**, 36-39 (1966).
9. Arlt, G., Hennings, D., & de With, G. Dielectric properties of fine-grained barium titanate ceramics, J. Appl. Phys. **58**, 1619-1625 (1985).
10. Hoshina, T. Takizawa, K. Li, J. Kasama, T. Kakemoto, H. & Tsurumi, T. Domain size effect on dielectric properties of barium titanate ceramics, J. J. Appl. Phys. **47**, 7607-7611 (2008).

11. Hoshina, T., Kigoshi, Y., Hatta, S., Takeda, H. & Tsurumi, T. Domain contribution to dielectric properties of fine-grained $BaTiO_3$ ceramics, J. J. Appl. Phys. **48**, 09KC01 (2009).
12. Cao, W. & Randall, C. A. Grain size relations in bulk ceramic ferroelectric materials, J. Phys. Chem. Solids, **57**, 1499-1505 (1996).
13. Buscaglia, V. Et al. Grain size and grain boundary-related effects on the properties of nanocrystalline barium titanate ceramics, J. Eur. Ceram. Soc. **26**, 2889-2898 (2006).
14. Polotai, V. A., Ragulya, V. A. & Randall, C. A. Preparation and size effect in pure nanocrystalline barium titanate ceramics, Ferroelectrics, **288**, 93-102 (2003).
15. Fujii, I., Ugorek, M. & Trolier-McKinstry, S. Grain size effect on the dielectric nonlinearity of $BaTiO_3$ ceramics, J. Appl. Phys. **107**, 104116 (2010).
16. Kinoshita, K. & Yamaji, A. Grain size effects on dielectric properties in barium titanate ceramics, J. Appl. Phys. **47**, 371-373 (1976).
17. Bell, A. J. Grain size effects in barium titanate – revisited, Proceedings of the 9th IEEE ISAF meeting, 14-17 (1994).
18. Hoshina, T. Kigoshia, Y. Hatta, S. Teranishi, T. Takeda, H. & Tsurumi, T. Size effect and domain-wall contribution of barium titanate ceramics, Ferroelectrics **402**, 29-36 (2010).
19. Arlt, G. & Peusens, H. The dielectric constant of coarse grained $BaTiO_3$ ceramics, Ferroelectrics, **48**, 213-224 (1983).
20. Miclea, C. et al. Microstructure and properties of barium titanate ceramics prepared by mechanochemical synthesis, Romanian J. Info. Sic. Tech. **10**, 335-345 (2007).
21. Takahashi, H., Numamoto, Y., Tani, J., & Tsurekawa, S. Piezoelectric properties of $BaTiO_3$ ceramics with high performance fabricated by microwave sintering, J. J. Appl. Phys. **45**, 7405-7408 (2006).

22. Bell, A. J., Moulson, A. J., & Cross, L. E. The effect of grain size on the permittivity of $BaTiO_3$, Ferroelectrics **54**, 147 (1984).

23. Subbarao, E. C., McQuarrie, M. C. & Buessem, W. R. Domain effects in polycrystalline barium titanate, J. Appl. Phys. **28**, 1194-200 (1957).

24. Hoffmann, M. J., Hammer, M., Endriss, A. & Lupascu, D. C. Correlation between microstructure, strain behavior, and acoustic emission of soft PZT ceramics, Acta Mater. **49**, 1301-1310 (2001).

25. Hall, D. A., Steuwer, A., Cherdhirunkorn, B., Mori, T. & Withers, P. J. A high energy synchrotron X-ray study of crystallographic texture and lattice strain in soft lead zirconate titanate ceramics, J. Appl. Phys. **96**, 4245–4252 (2004).

26. Jones, J. L., Slamovich, E. B. & Bowman, K. J. Domain texture distributions in tetragonal lead zirconate titanate by X-ray and neutron diffraction, J. Appl. Phys. **97**, 034113 (2005).

27. Kungl, H. et al. Estimation of strain from piezoelectric effect and domain switching in morphotropic PZT by combined analysis of macroscopic strain measurements and synchrotron X-ray data, Acta Mater. **55**, 1849-1861 (2007).

28. Jones, J. L., Pramanick, A. & Daniels, J. E. High-throughput evaluation of domain switching in piezoelectric ceramics and applications to $PbZr_{0.6}Ti_{0.4}O_3$ doped with La and Fe, Appl. Phys. Lett. **93**, 152904 (2008).

29. Daniels, J. E., Jo, W., Rödel, J., Honkimäi, V. & Jones, J. L. Electric-field-induced phase-change behavior in $(Bi_{0.5}Na_{0.5})TiO_3$-BaTiO3-$(K_{0.5}Na_{0.5})NbO_3$: A combinatorial investigation, Acta Mater. **58**, 2103-2111 (2010).

30. Pramanick, A., Damjanovic, D., Daniels, J. E., Nino, J. C. & Jones, J. L. Origins of electro-mechanical coupling in polycrystalline ferroelectrics during subcoercive electrical loading, J. Am. Ceram. Soc. **94**, 293–309 (2011).

31. Jones, J. L. Aksel, E. Tutuncu, G. Usher, T.-M. Chen, J. Xing, X. & Studer, A. J. Domain wall and interphase boundary motion in a two-phase morphotropic phase boundary ferroelectric: frequency dispersion and contribution to piezoelectric and dielectric properties, Phys. Rev. B **86**, 024104 (2012).

32. Ghosh, D., Han, H., Nino, J. C., Subhash, G., & Jones, J. L. Synthesis of $BaTiO_3$-20wt%$CoFe_2O_4$ nanocomposites via spark plasma sintering, J. Am. Ceram. Soc. **95**, 2504-2509 (2012).

33. Yoon, S. et al. Spark plasma sintering of nanocrystalline $BaTiO_3$- powders: consolidation behavior and dielectric characteristics, J. Eur. Ceram. Soc. **31**, 1723–1731 (2011).

34. Arlt, G. The role of domain walls on the dielectric, elastic and piezoelectric properties of ferroelectric ceramics, Ferroelectrics **76**, 451-458 (1987).

35. Frey, M. H. & Payne, D. A. Grain-size effect on structure and phase transformations for barium titanate, Physical Review B **54**, 3158-3168 (1996).

36. Wada, S., Yako, K., Kakemoto, H., Tsurumi, T. & Kiguchi, T. Enhanced piezoelectric properties of barium titanate single crystals with different engineered-domain sizes. J. Appl. Phys. **98**, 014109 (2005).

37. Arlt, G. & Pertsev, N. A. Force constant and effective mass of 90° domain walls in ferroelectric ceramics, J. Appl. Phys. **70**, 2283-2289 (1991).

38. Pertsev, N. A & Arlt, G. Forced translational vibrations of 90° domain walls and the dielectric dispersion in ferroelectric ceramics, J. Appl. Phys. **74**, 4105-4112 (1993).

39. Demartin, M. & Damjanovic, D. Dependence of the direct piezoelectric effect in coarse and fine grain barium titanate ceramics on dynamic and static pressure, Appl. Phys. Lett. **68**, 3046-3048 (1996).

40. Arlt, G. Review twinning in ferroelectric and ferroelastic ceramics: stress relief, J. Mater. Sci. **25**, 2655-2666 (1990).

41. Jacobs, A. E. Phys. Rev. B Solitons of the square-rectangular martensitic transformation, **31**, 5984-5989 (1985).

42. Daniels, J. E., Jones, J. L. & Finlayson, T. R. Characterization of domain structures from diffraction profiles in tetragonal ferroelastic ceramics, J. Phys. D: Appl. Phys. **39**, 5294-5299 (2006).

43. Yen, F.-S., Hsiang, H.-I & Chang, Y.-H. Cubic to tetragonal phase transformation of ultrafine $BaTO_3$ crystallites at room temperature, J. J. Appl. Phys. **34**, 6149-6155 (1995).

44. Huang, T.-C., Wang, M.-T., Sheu, H.-S. & Hsieh, W.-F. Size-dependent lattice dynamics of barium titanate nanoparticles, J. Phys.: Condens. Matter. **19**, 476212-(2007).

45. Tutuncu, G., Damjanovic, D., Chen, J. & Jones, J. L. Deaging and asymmetric energy landscapes in electrically biased ferroelectrics, Phys. Rev. Letts. **108**, 177601 (2012).

46. Merz, W. J. Double hysteresis loop of $BaTiO_3$ at the Curie point, Phys. Rev. **91**, 513-517 (1953).

47. Meyerhofer, D. Transition to the ferroelectric state in barium titanate, Phys. Rev. **112**, 413-423 (1958).

48. Picht, G., Kungl, H., Bäurer, M. & Hoffmann, M. J. High electric field induced strain in solid-state route processed barium titanate ceramics, Func. Mater. Letters. **3**, 59-64 (2010).

49. Cao, H. Devreugd, C. P. Ge, W., Li, J. Viehland, D. Luo, H. & Zhao, X. Monoclinic M_C phase in (001) field cooled BaTiO3 single crystals, Appl. Phys. Lett. **94**, 032901 (2009).

50. Yoshimura, Y. Kojimab, A. Tokunaga, N. Tozaki, K. & Koganezawa, T. New finding of coherent hybrid structure of $BaTiO_3$ single crystal in the room temperature phase, Phys. Letts. A **353**, 250-254 (2006).

51. Pramanick, A., Damjanovic, D., Nino, J. C. & Jones, J. L. Subcoercive cyclic electrical loading of lead zirconate titanate ceramics I: nonlinearities and losses in the converse piezoelectric effect, J. Am. Ceram. Soc. **92**, 2291-2299 (2009).

52. Pramanick, A., Daniels, J. & Jones, J. L. Subcoercive cyclic electrical loading of lead zirconate titanate ceramics II: time-resolved X-ray diffraction, J. Am. Ceram. Soc. **92**, 2300-2310 (2009).

53. Jones, J. L., Daniels, J. E., Studer, A. J. & Hoffman, M. Direct measurement of the domain switching contribution to the dynamic piezoelectric response in ferroelectric ceramics, Appl. Phys. Lett. **89**, 092901 (2006).

54. Cross, L. E. Ferroelectric ceramics: tailoring properties for specific applications, Ferroelectric Ceramics, 1-85, Ed. Setter, N. & Colla, E. L. (Basel: Birkhäuser) (1993).

55. Damjanovic, D. Ferroelectric, dielectric and piezoelectric properties of ferroelectric thin films and ceramics, Rep. Prog. Phys. **61** 1267–1324 (1998).

56. Zhang, Q. M. Pan, W. Y. Jang, S-J. & Cross, L. E. Domain wall excitations and their contributions to the weak signal response of doped lead zirconate titanate ceramics, J. Appl. Phys. **64**, 6445-6451 (1988).

57. Zhang, Q. M. Wang, H. Kim, N. & Cross, L. E. Direct evaluation of domain wall and intrinsic contributions to the dielectric and piezoelectric response and their temperature dependence on lead zirconate titanate ceramics, J. Appl. Phys. 75, 454-459 (1994).

58. Hagemann, H. Loss mechanisms and domain stabilisation in doped BaTiO3, J. Phys. C: Solid State Phys. 11 3333-3344 (1978).

59. Damjanovic, D. Stress and frequency dependence of the direct piezoelectric effect in ferroelectric ceramics, J. Appl. Phys. **82**, 1788-1797 (1997).

60. Damjanovic, D. & Demartin, M. Contribution of the irreversible displacement of domain walls to the piezoelectric effect in barium titanate and lead zirconate titanate ceramics, J. Phys: Condens Matter, **9**, 4943-4953 (1997).

61. Bondarenko, E. I. Topolov, V. Y. & Turik, A. V. The role of 90° domain wall displacements in forming physical properties of perovskite ferroelectric ceramics, Ferroelectric Letts. Sec. **13**, 13-19 (1991).

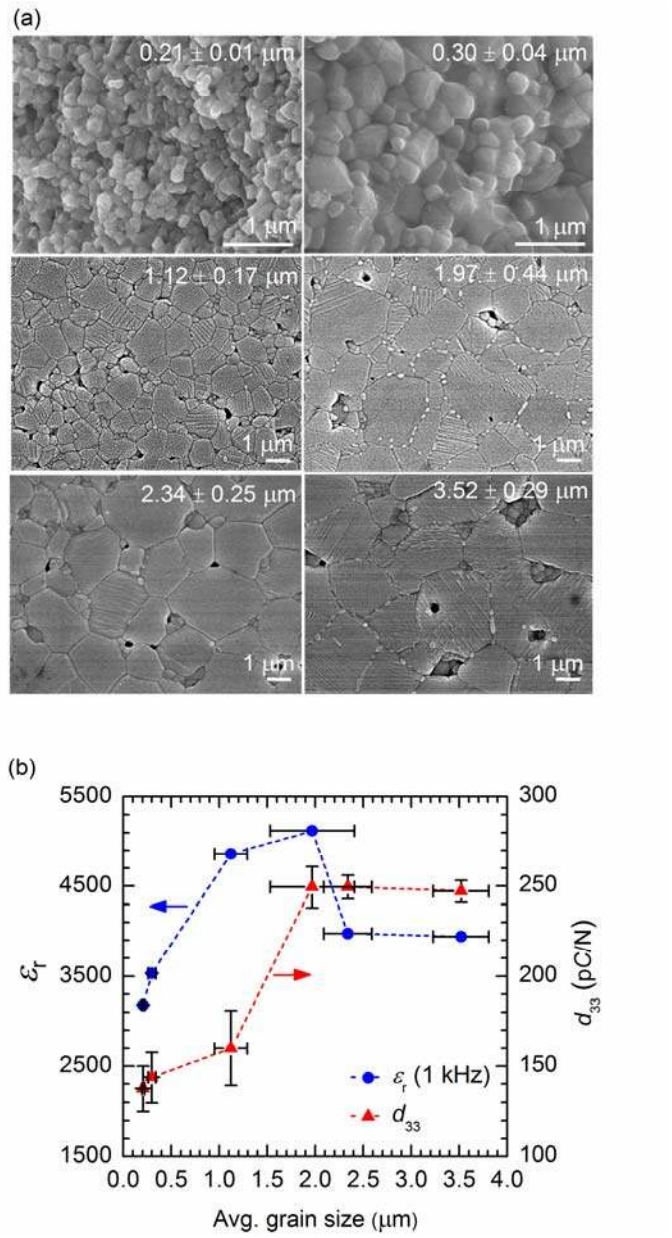

Figure 1: (a) Microstructures of BT of different grain sizes and (b) relative permittivity and longitudinal piezoelectric coefficient measurements.

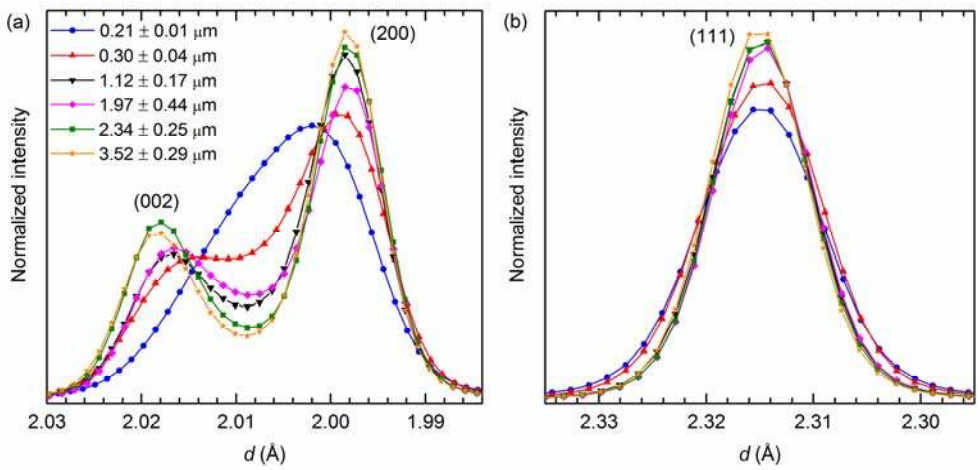

Figure 2: High-energy X-ray patterns of (a) {200} and (b) (111) Bragg reflections prior to electric field application.

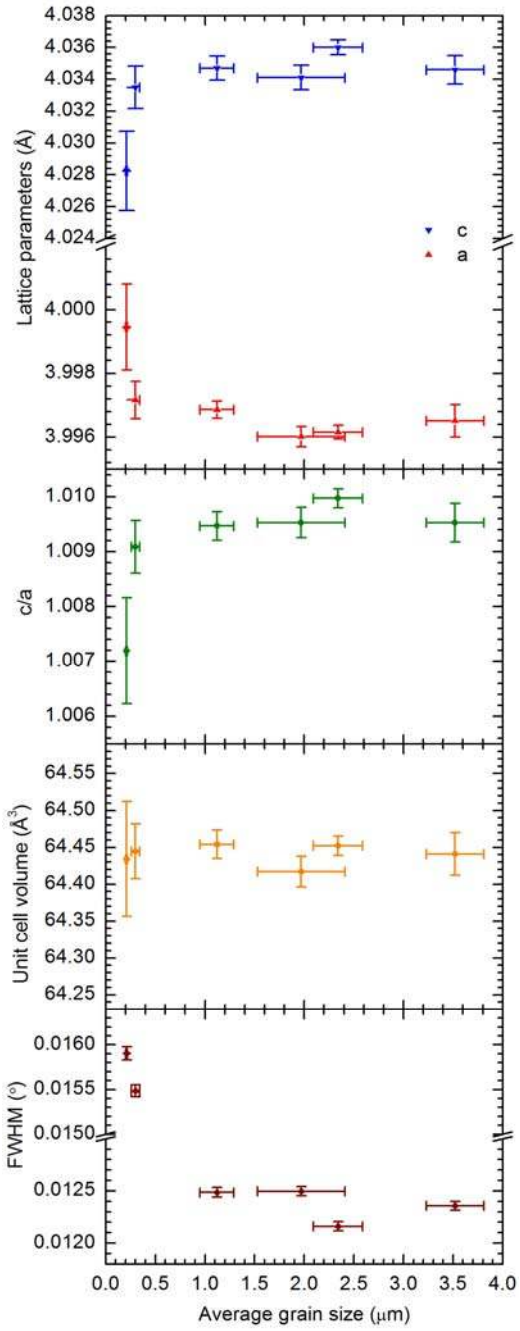

Figure 3: Variation in (a) tetragonal lattice parameters (*c* and *a*), (b) *c*/*a*, (c) unit cell volume, and (d) FWHM of (111) Bragg reflection as a function of average grain size of the synthesized $BaTiO_3$ samples.

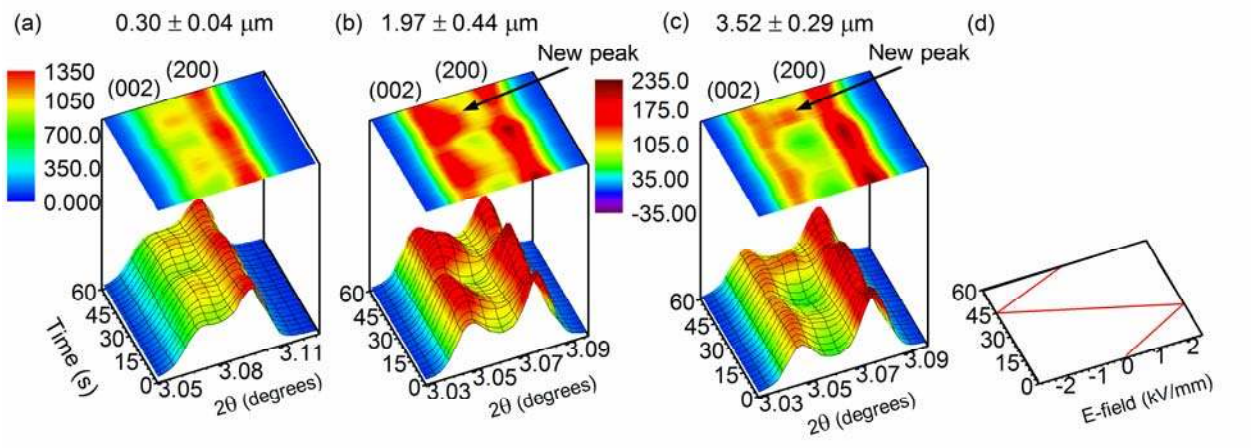

Figure 4: Contour plots of changes in intensities of (002) and (200) reflections during high electric field application (±2.5 kV/mm) revealing variation in 90° domain wall motion for (a) 0.3 μm), (b) ~2 μm and (c) ~3.5 μm grain sizes of $BaTiO_3$.

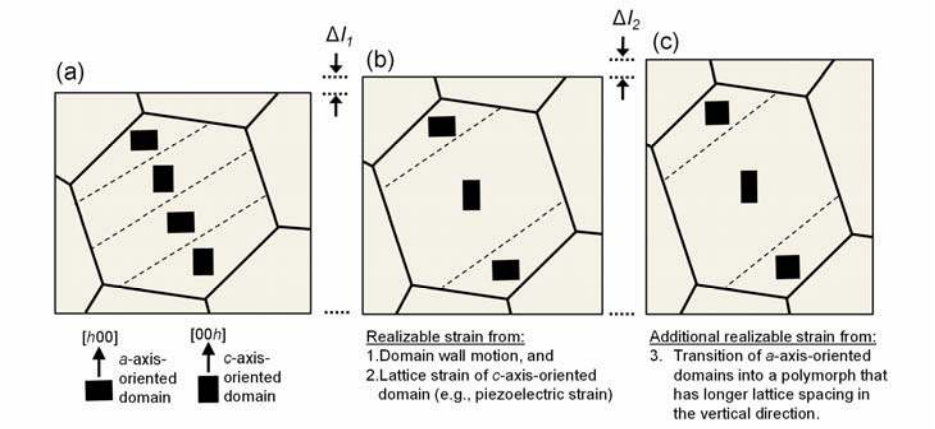

Figure 5: Simplified illustration of an electromechanical strain mechanism in which a-axis oriented domains transform into a new polymorph in order to facilitate strain of a crystalline grain. In the initial state (a), the black rectangles represent domain orientation states within a single representative grain that are separated by domain walls. In (b), strain is achieved through domain wall motion and distortion of the unit cells (e.g., piezoelectric strain). In (c), additional strain is enabled from the phase transition mechanism.

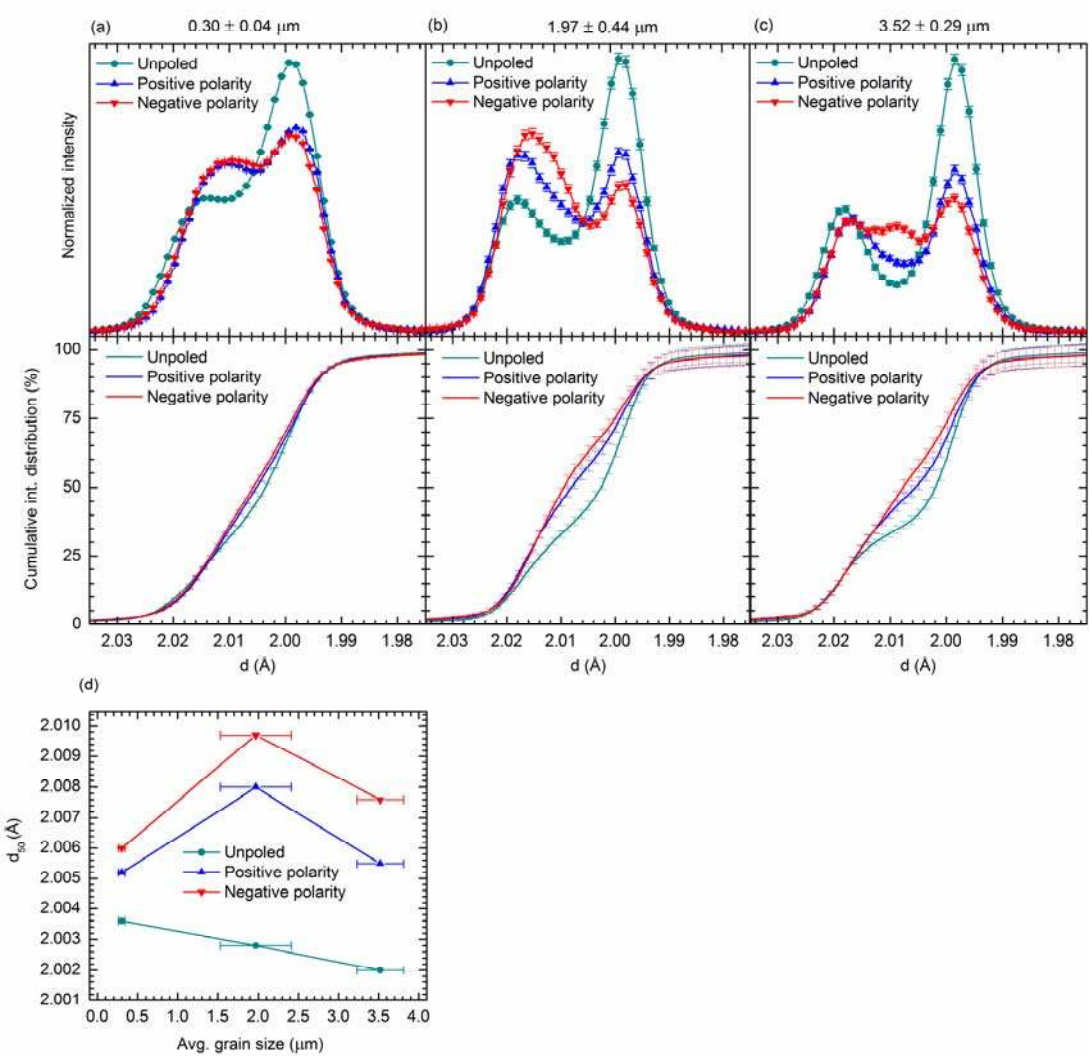

Figure 6: Cumulative diffraction intensity distribution of interplanar spacing, *d*, across the {002} diffraction profile for (a) 0.3 μm, (b) ~2 μm and (c) ~3.5 μm grain sizes of $BaTiO_3$ prior to and during application of strong electric field amplitudes (both the positive and negative polarities). (d) Calculated d_{50} values as a function of grain size.

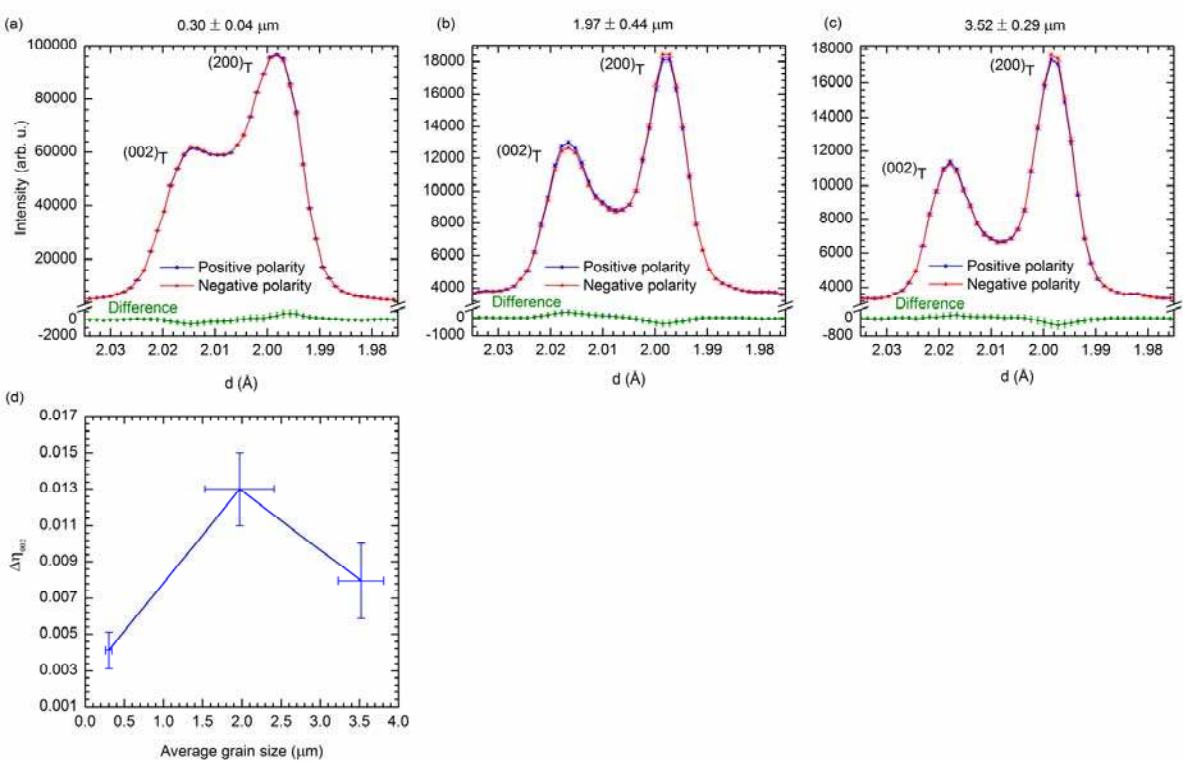

Figure 7: XRD profiles of (002) and (200) Bragg reflections during application of weak (subcoercive) electric field amplitudes (±0.2 kV/mm) revealing variation in 90° domain wall motion for (a) 0.30 μm), (b) 1.97 and (c) 3.52 μm grain sizes of $BaTiO_3$. (d) Calculated values of domain switching as a function of grain size.

Supporting Information for

Domain wall displacement is the origin of superior permittivity and piezoelectricity in $BaTiO_3$ at intermediate grain sizes

Dipankar Ghosh,[1,3] Akito Sakata,[1] Jared Carter,[1] Pam A. Thomas,[4] Hyuksu Han,[1] Juan C. Nino[1] and Jacob L. Jones[1,2]

[1]*Department of Materials Science and Engineering, University of Florida, Gainesville, FL 32611, USA*

[2]*Department of Materials Science and Engineering, North Carolina State University, Raleigh, NC, 27695, USA*

[3]*Division of Engineering and Applied Science, California Institute of Technology, Pasadena, CA 91125, USA*

[4]*Department of Physics, University of Warwick, Coventry, CV4 7AL, UK*

Procedures and Materials

Materials synthesis

For samples sintered via spark plasma sintering (SPS), 5 g of powder was placed in a 20 mm graphite die and sintered in an SPS system (Dr. Sinter 1020). During sintering, the sample was: (i) first heated from room temperature to 600°C at a rate of 200°C/min, then (ii) heated from 600 to 900°C (the sintering temperature) at a rate of 50°C/min, (iii) held at 900°C for 5 min, and finally (iv) cooled to room temperature at a rate of 100°C/min. The maximum voltage and current were 4 V and 800 Amp, respectively. Sintering was performed under an applied uniaxial pressure was 60 MPa. A portion of this SPS $BaTiO_3$ pellet was heated to 1000°C for 6 hours for grain growth. For conventional sintering, green pellets (diameter 10 mm and thickness 2 mm) were made initially in a uniaxial press using a steel die and then isostatically pressed at a pressure of 225 MPa. The green pellets were then (i) heated from room temperature to the sintering temperature at a rate of 5°C/min, (ii) held at the sintering temperature for 120 min and (iii) finally cooled to room temperature at a rate of 5°C/min.

For samples sintered via pressureless sintering (PS), four different sintering temperatures (1200°C, 1225°C, 1250°C, 1275°C) were selected such that $BaTiO_3$ ceramics can be synthesized with comparable density but with different grain sizes. $BaTiO_3$ is known to undergo partial reduction when sintered in non-oxidizing atmosphere (e.g., vacuum) and/or at high temperature [1,2]. Additionally, the use of a graphite die in the SPS may cause diffusion of carbon from the graphite die to the surfaces of the sintered materials and also result in reduction of $BaTiO_3$. Therefore, a post-sintering heat treatment procedure was employed (here after referred as air annealing) where all the sintered materials were further heated to 800°C and held for 6 hours in a tube furnace under an atmosphere of flowing oxygen (MTI Corporation, Richmond, California)

to remove the carbon from the surfaces of the samples (sintered by SPS) and re-oxidize the $BaTiO_3$ grains. All the sintering and post-sintering heat treatment schemes are listed in Table S1.

Microstructures

Microstructures of the sintered materials were imaged using scanning electron microscopy (SEM) (6335F FEG-SEM). Sintered $BaTiO_3$ specimens were first ground using 800 grit silicon carbide paper. The ground surfaces were next polished using a 0.5 μm alumina slurry and final polishing was done using a 0.04 μm colloidal silica slurry. Thermal etching was then used to reveal the microstructure on the polished surfaces. For the $BaTiO_3$ ceramics synthesized by SPS, no suitable thermal etching temperature was found. This is because thermal treatment could not exceed 900°C (the SPS sintering temperature) because grain growth would occur and thermal treatment below 900°C did not result any etching of the polished sample surfaces. For these materials, therefore, the average grain sizes were measured from the SEM micrographs of the fractured surfaces. For $BaTiO_3$ ceramics sintered at 1200°C and 1225°C by conventional sintering, thermal etching was performed at 1050°C for 1 hour whereas for $BaTiO_3$ ceramics sintered at 1250 and 1275°C, thermal etching was conducted at 1100°C for 1 hour. All the thermal etching treatments were conducted in a box furnace in air. As mentioned in the experimental section, the lineal intercept technique in accordance with the ASTM E112-10 standard was used to determine the average grain sizes of the sintered $BaTiO_3$ ceramics. Figure S2 shows grain size distributions of all synthesized $BaTiO_3$ materials. All the conditions for thermal etching treatments and measured values of grain sizes are given in Table S2.

Specimen preparation for dielectric and piezoelectric

For dielectric and piezoelectric measurements, thin layers of gold (Au) were first deposited on two parallel surfaces of the annealed $BaTiO_3$ specimens via sputter deposition, after

which silver paste was applied on top of the Au. The silver paste was dried in air for 5 min. All dielectric and piezoelectric data measured on annealed $BaTiO_3$ samples are summarized in Table S2.

High-energy, in situ XRD measurements

For *in situ*, high-energy XRD measurements, smaller specimens of dimensions of 1 mm x 1 mm x 5 mm were cut from the larger sintered samples using a diamond saw, all the sides of the samples were polished, and samples were annealed at 300°C for 3 hours. Two of the parallel and opposing 1 mm x 5 mm surfaces of each sample were electroded using a silver paste.

All the XRD measurements were completed using an X-ray beam size of 0.2 mm x 0.2 mm and two-dimensional diffraction images were collected with a Perkin Elmer amorphous silicon area detector positioned in the forward direction (transmission geometry) at a distance of 2248 mm. A schematic of the experimental geometry and front view of the area detector image are shown in Fig. S3, where φ defines the azimuthal angle on the detector. At a value of φ=0°, the detector measures plane normals that are approximately parallel to the applied electric field and a value of φ = 90° corresponds to the perpendicular direction with to the applied electric field (Figure S2). From the two-dimensional diffraction images, segments of the ring patterns were integrated using the software package Fit2d [3] to obtain one-dimensional diffraction patterns. In the present work, ring patterns were integrated over an azimuthal angle of 15º (7.5º on each side of the direction parallel to the applied electric field).

Determination of the extent of 90º domain reorientation

In tetragonal ferroelectrics, 90º domain wall motion can be observed and quantified from the changes in the changes in the volume fractions of the (002) and (200) orientation variants

during electric field application. However, due to evolution of an additional phase during high electric field application in $BaTiO_3$, a new method was used that associates changes in the {002} diffraction profile with the macroscopic strain of the sample. For this purpose, a cumulative diffraction intensity distribution of interplanar spacing, *d*, across the {002} diffraction profile was used and the method has been described in the main text.

For the weak electric field measurements in which no field-induced secondary polymorph is observed, the 90º domain wall motion was calculated from the changes in the volume fractions of the (002) and (200) orientation variants. In perovskite ferroelectrics with a tetragonal crystal structure, the volume fraction of the material with (002) domains parallel to a particular direction of specimen is given by [4]:

$$\mathrm{v}_{002} = \frac{\frac{\mathrm{I}_{002}}{I'_{002}}}{\frac{\mathrm{I}_{002}}{I'_{002}} + 2\left(\frac{\mathrm{I}_{200}}{I'_{200}}\right)} \tag{S.1}$$

where I_{002} is the integrated area of the *(hkl)* Bragg peak for a given sample with a preferred orientation of 90º domains and I'_{hkl} is the integrated area of the same Bragg peak for a sample where 90º domains have no preferred orientations [4]. In a sample with random orientation of 90º domains, the value of v_{002} is equal to 1/3. Therefore, during electric field application, the volume fraction of the (002) domains (η_{002}) that has been reoriented in the direction of the applied field is given by [4]

$$\eta_{002} = \mathrm{v}_{002} - \frac{1}{3}. \tag{S.2}$$

If η^{+}_{002} and η^{-}_{002} represent the volume fractions of the 002 domains oriented in a particular direction during the positive and negative electric field cycles (bipolar electric field for subcoercive measurements) respectively, then the volume fraction of the (002) domains that are

reoriented in a specific sample direction ($\Delta\eta_{002}$) is expressed relative to the maximum and minimum values through [5],

$$\Delta\eta_{002} = \eta_{002}^{+} - \eta_{\bar{0}02}^{-} . \quad \text{(S.3)}$$

References

1. Ghosh, D., Han, H., Nino, J. C., Subhash, G., & Jones, J. L. Synthesis of $BaTiO_3$-20wt%$CoFe_2O_4$ nanocomposites via spark plasma sintering, J. Am. Ceram. Soc. **95**, 2504-2509 (2012).
2. Yoon, S. et al. Spark plasma sintering of nanocrystalline $BaTiO_3$- powders: consolidation behavior and dielectric characteristics, J. Eur. Ceram. Soc. **31**, 1723–1731 (2011).
3. Hammersley, A. P. Fit2D. 1987, ESRF: Grenoble, France (fit2d_12_077_i686_WXP).
4. Pramanick, A., Damjanovic, D., Daniels, J. E., Nino, J. C. & Jones, J. L. Origins of electro-mechanical coupling in polycrystalline ferroelectrics during subcoercive electrical loading, J. Am. Ceram. Soc. **94**, 293–309 (2011).
5. Seshadri, S. B. Prewitt, A. D. Studer, A. J. Damjanovic, D. & Jones, J. L. An in situ diffraction study of domain wall motion contributions to the frequency dispersion of the piezoelectric coefficient in lead zirconate titanate, Appl. Phys. Letts. **102**, 042911 (2013).

Table S1: Sintering parameters and density measurements of $BaTiO_3$ ceramics by SPS and conventional sintering

Sintering technique	Sample ID	Sintering parameters			Annealing temp. (°C) and time (min)	Density g/cm^3 (%)
		Temp (°C)	Time (min)	Pressure (MPa)		
SPS	SPS_900	900	5	60	800, 360	5.7 (94.2)
	SPS_1000				1000, 360 and 800, 360	5.9 (98)
PS	PS_1200	1200	120	0	800, 360	5.7 (94.29)
	PS_1225	1225	120	0	800, 360	5.8 (97)
	PS_1250	1250	120	0	800, 360	5.8 (97)
	PS_1275	1275	120	0	800, 360	5.9 (97.6)

Table S2: Thermal etching conditions, grain size, and relative permittivity (ε_r), dielectric loss (tanδ), and piezoelectric coefficient (d_{33})

Sample ID	Thermal etching parameters		Average GS (µm)	Dielectric properties (1 KHz)		d_{33} (pC/N)
	Temp (°C)	Time (min)		ε_r/tanδ (RT)	ε_r/tanδ (C_T)	
SPS_900	---	---	0.21 ± 0.01	3236/0.08 (32°C)	5161/0.09 (126.1°C)	138 ± 13
SPS_1000	---	---	0.30 ± 0.04	3424/0.04 (31.7°C)	9252/0.04 (130.7°C)	144 ± 14
PS_1200	1050	60	1.12 ± 0.17	4436/0.06 (31.9°C)	8305/0.04 (129°C)	160 ± 21
PS_1225	1050	60	1.97 ± 0.44	4841/0.03 (32°C)	10029/0.02 (129°C)	249 ±12
PS_1250	1100	60	2.34 ± 0.25	3798/0.02 (31.6°C)	7812/0.01 (129.5°C)	250 ± 7
PS_1275	1100	60	3.52 ± 0.29	3799/0.02 (31.6°C)	9145/0.03 (129.9°C)	247 ± 6

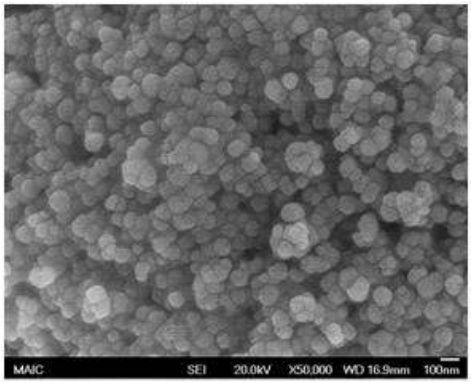

Figure S1. SEM micrograph of nanocrystalline $BaTiO_3$ powder.

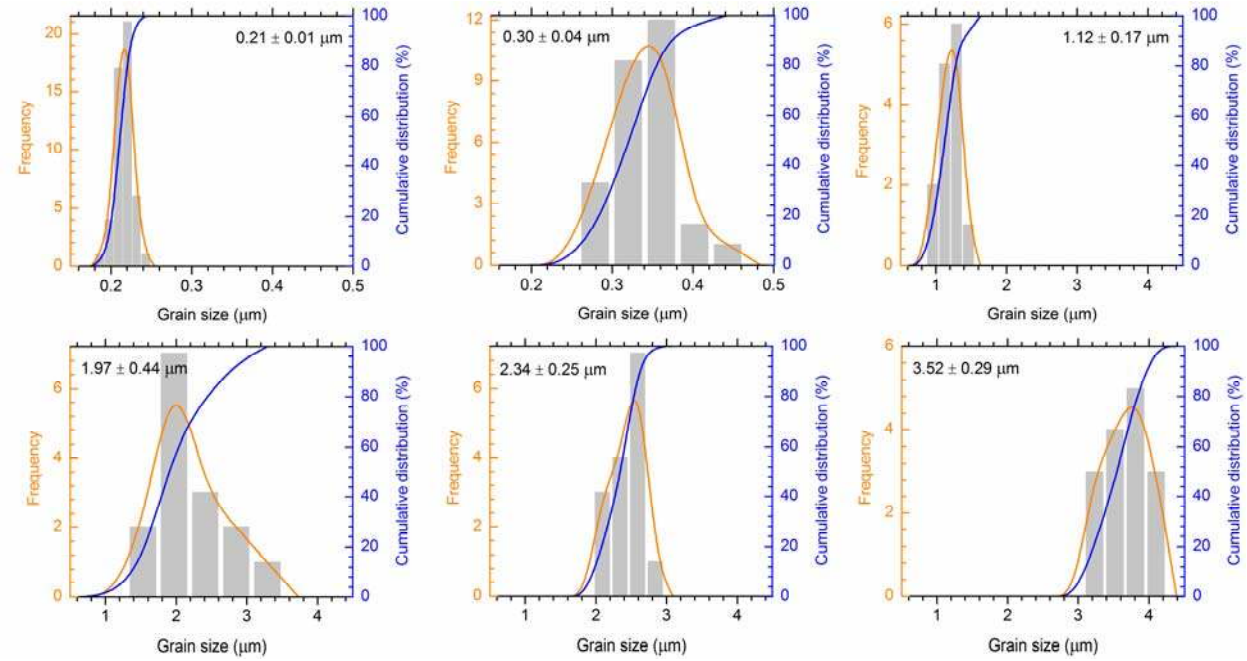

Figure S2: Grain size distributions of the synthesized $BaTiO_3$ ceramics.

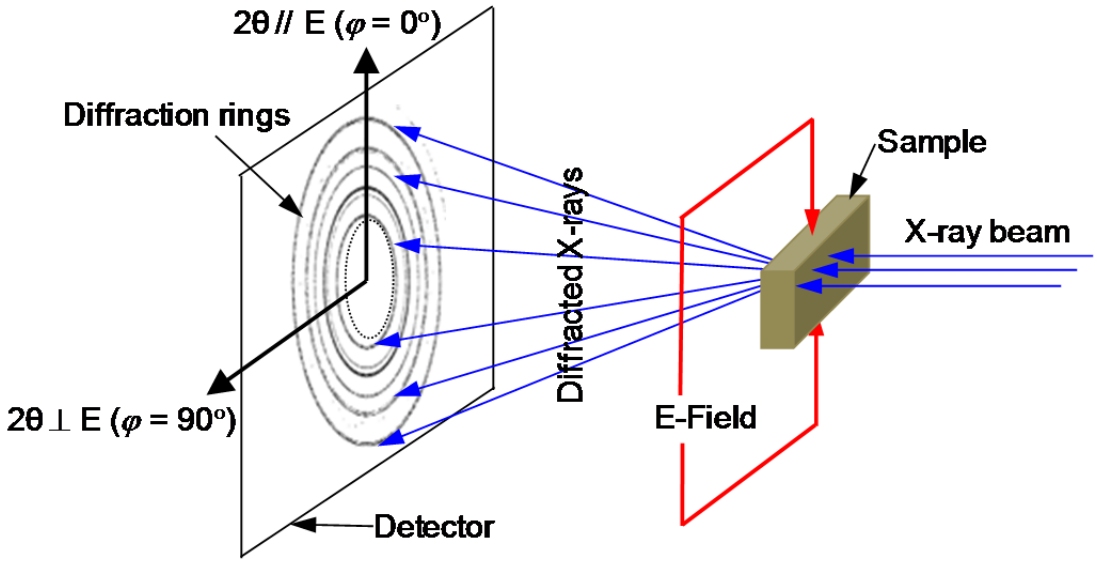

Figure S3: Schematic of experimental geometry and front view of detector image.

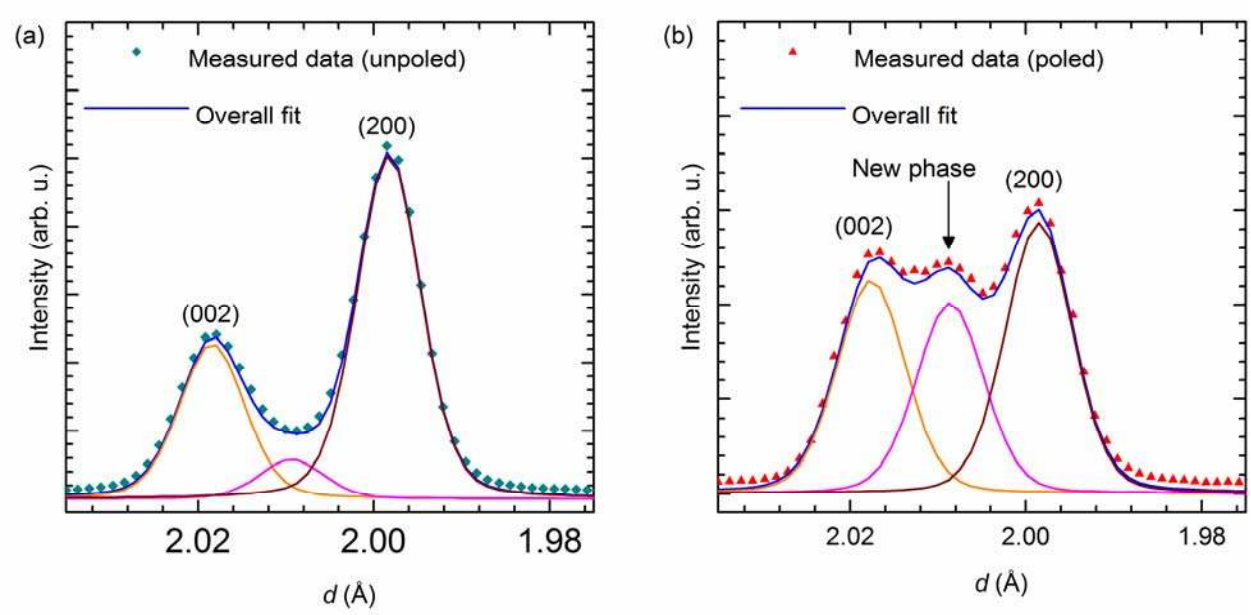

Figure S4: Representative fit of {200} reflections measured (a) prior electric field application and (b) during electric field application for the sample with a grain size of 3.52 µm using three symmetric pseudo-Voigt profile functions.

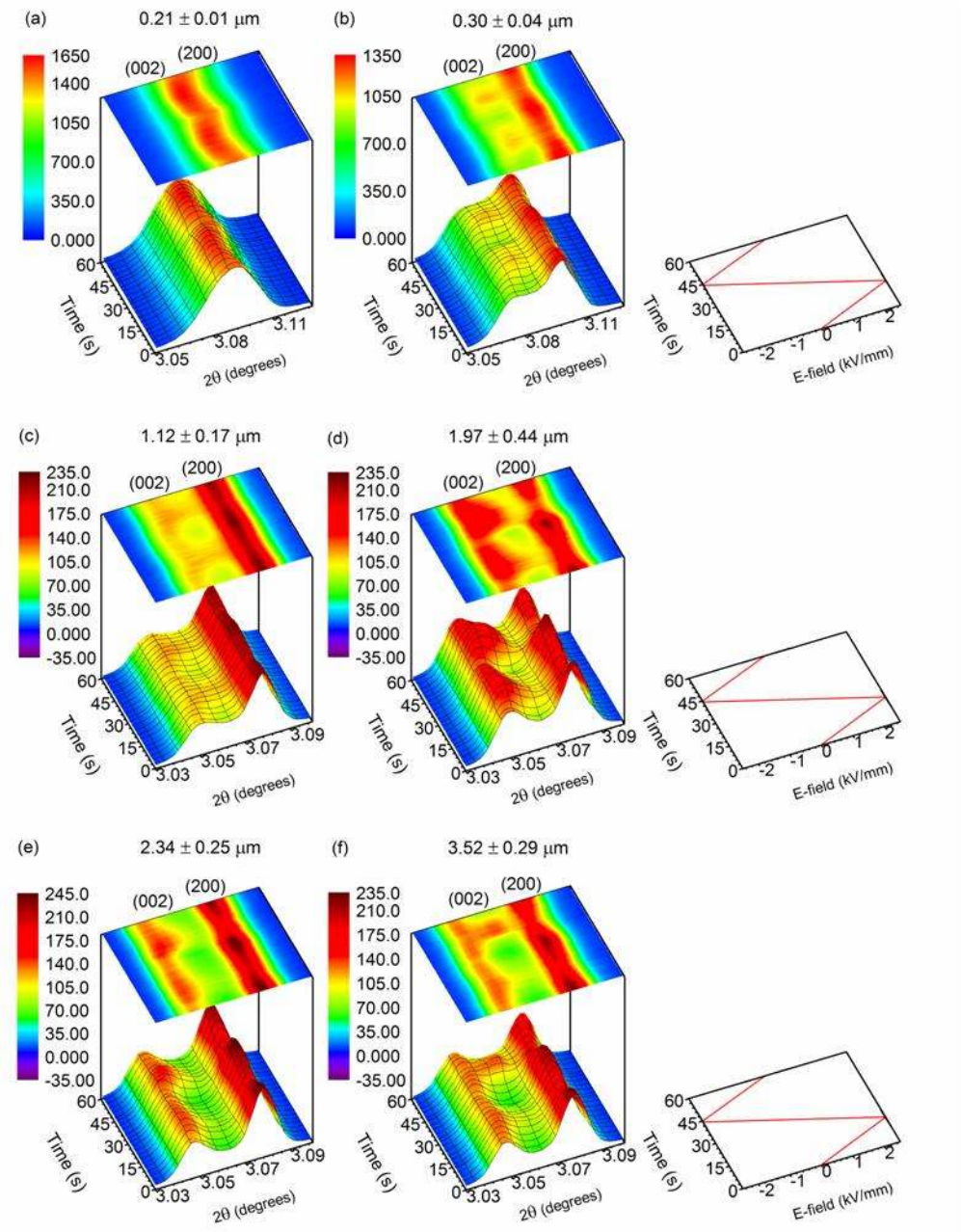

Figure S5: Contour plots of changes in intensities of {002} diffraction profile containing the (002) and (200) tetragonal phase reflections during electric field application (±2.5 kV/mm), revealing variation in extent of domain wall motion in various grain size $BaTiO_3$ ceramics.

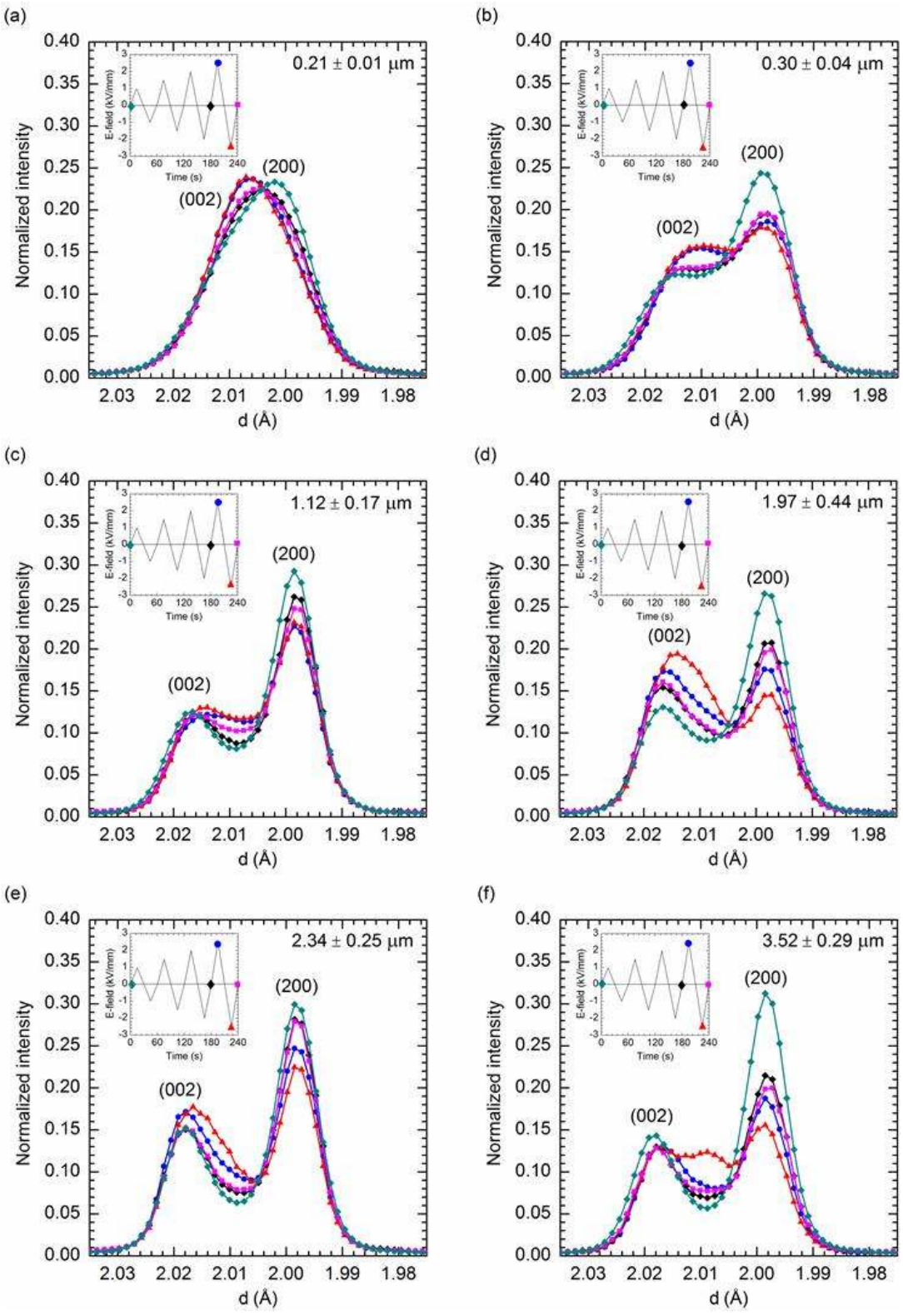

Figure S6: Selective XRD patterns measured prior and during electric field application (± 2.5 kV/mm) for all the grain sizes of $BaTiO_3$.

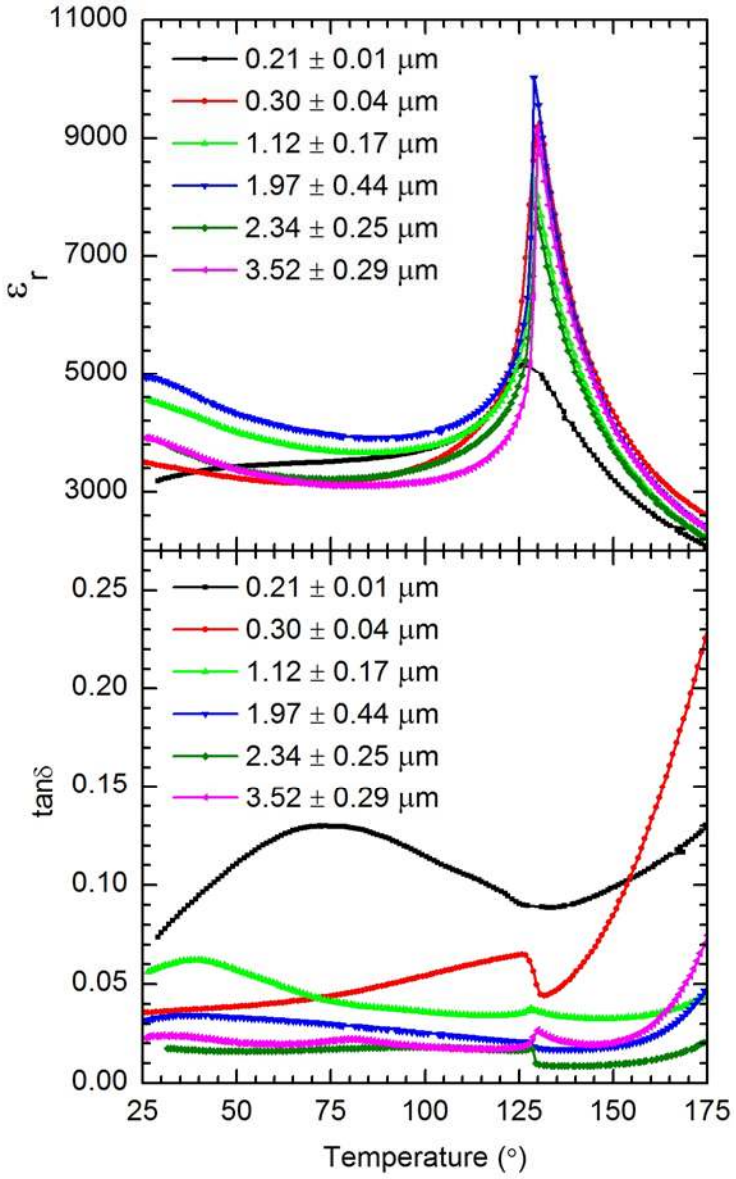

Figure S7: Dielectric permittivity and loss of the $BaTiO_3$ samples of different grain sizes as a function of temperature at 1 kHz.